1. Introduction

Aerosol Deposition (AD) is a unique thick film deposition technology that is capable of depositing ceramic, metallic, or composite films through the acceleration, impact and consolidation of dry, fine sized (~0.1-1μm) particle feedstock delivered by a carrier gas towards a substrate [akedo]. The use of fine particle feedstock is necessary in order for typically brittle materials (i.e., ceramics) to exhibit sufficient plasticity and non-brittle fracturing that is the key mechanism to coating consolidation [Sarobol], resulting in a dense, nano-crystalline grain size deposition.

One of the most notable attributes of the AD process is that coating deposition occurs at room temperature, with no thermal input to the feedstock or substrate necessary. As such, AD has garnered considerable interest as a method for deposition of functional ceramics, such as piezo-electrics [refs], ferro/para- magnetics [refs], and high permittivity dielectrics [ref]. This is driven by AD's ability to preserve feed stock stoichiometry in a deposited film, produce dense microstructures, and the ability to mate materials with vastly different melting temperatures or thermal expansion coefficients.

$BaTiO_3$ (and its derivatives) is a ceramic material that has been the subject of several studies using AD [refs], owing to its ability to be readily deposited by the AD process and the typically high dielectric constant observed in the bulk material. However, the dielectric constant of $BaTiO_3$ is highly dependent on its grain size when in the range of <500nm [ref Aygun, Kinoshita, Yamaji 1976 - Grain-Size Effects on Dielectric Properties in Barium-Titanate Ceramics]. Several experiments showed that post-deposition annealing used to increase the grain sizes within the AD $BaTiO_3$ film causes an increase in the permittivity with respect to the increasing grain size [3-5 jesses.]. With the nano-crystallinity commonly observed in as-deposited AD films, it becomes necessary to understand grain growth behavior of $BaTiO_3$ using post deposition heat treatment.

In addition to understanding the coating microstructure in the as-deposited state and its evolution through post-processing, residual stress in the as-deposited and post-processed films is an important factor to consider when mating dissimilar materials and exploring the integration of AD films into functional electrical components. Previous studies have presented residual film stresses of $BaTiO_3$ and other materials deposited by AD [refs], showing compressive residual stresses within the film due to the high velocity particle impact used for coating formation. However, to date there has been no study of the behavior of film stress generation *in-situ* during the deposition process, where changes in the deposition behavior of successive AD layers have been reported in literature [refs]. As a room temperature process, thermal expansion coefficient mismatch between the coating and substrate is not expected to have a role in the film residual stress from deposition. However, post-deposition annealing can alter the residual stresses in AD films [Kawakami, Watanabe et al 2016 - Effects of substrate materials on piezoelectric properties of BaTiO3 thick films]

2. Experimental Methods

2.1 Film Deposition

A schematic of the AD process is shown in **Error! Reference source not found.**. Dry (<2ppm H_2O) compressed air was used as the carrier gas with commercially available HPB-4000 $BaTiO_3$ powder [Nanoxide, Albuquerque NM]. The aerosol of $BaTiO_3$ powder and air was generated using an RBG 1000 ID [Palas, Karlsruhe, Germany], a rotating brush aerosol generator, to ensure a consistent and homogenous powder feed. The aerosol was introduced into vacuum through a micro-abrasive nozzle [Comco Inc., Burbank CA] with a 2.0mm nozzle opening. Substrates were translated with an XY stage while maintaining a spray distance of 5mm. A schematic of the AD system and SEM micrographs of the feedstock powder and deposited film surface are shown in Figure 1

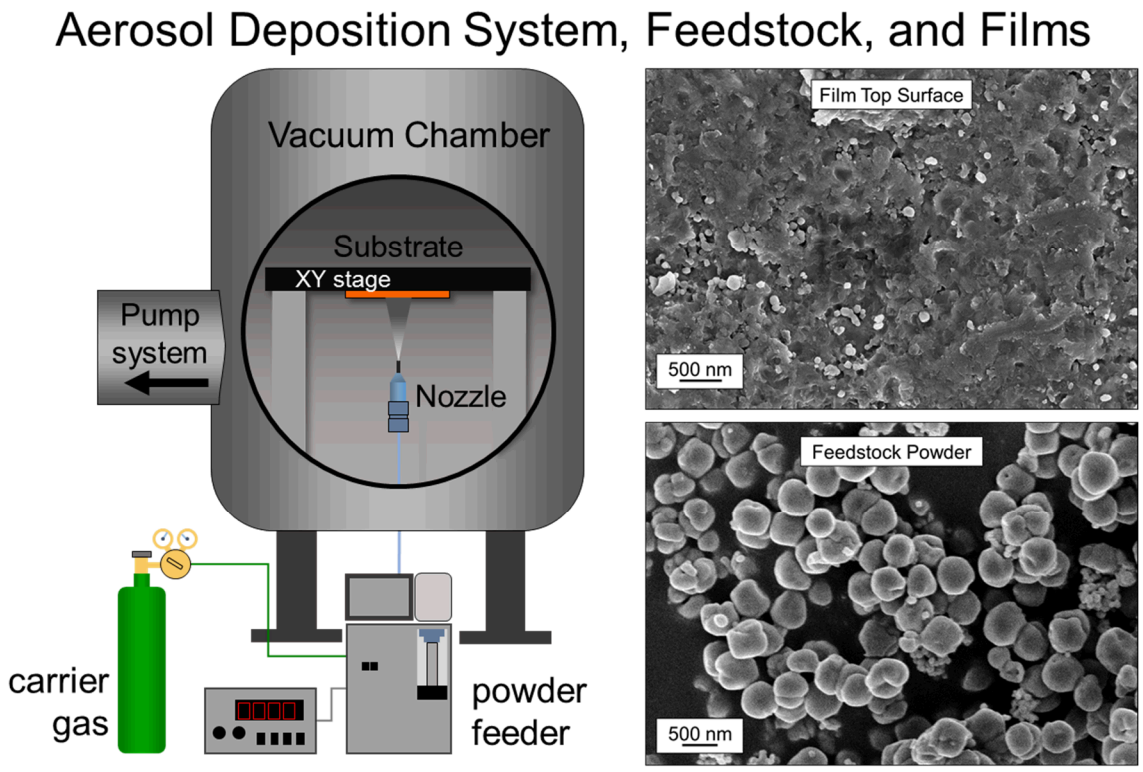

Figure 1: Aerosol Deposition system and SEM micrographs of the feedstock powder and deposited film surface

Pressure at the output of the aerosol generator was measured to be ~940 Torr with the vacuum chamber measured ~0.5 Torr. Powder was fed into the aerosol generator at a constant rate using a 14mm diameter cylinder of lightly packed powder at a longitudinal rate of 60mm/hr. This volumetric displacement calculates to a maximum feed rate of 0.93 g/min, though with imperfect powder packing a lower mass feed rate is expected. A substrate translation speed of 1200mm/min and pitch of 0.5mm between scans was used for sample preparation.

AD BaTiO3 films of approximately 12-13µm thickness were deposited onto (0001) sapphire substrates with an area of 10mm x 10mm each for heat treatment, X-ray diffraction, and TEM studies. Additional films of 3-4µm thickness were deposited onto soda lime glass substrates with

an area of 12mm x 60mm. The edges of the glass substrates were held against cylindrical edges in order to allow free bending of the substrate during deposition and center point deflection of the substrate was monitored during deposition using an HL-G1 Compact Laser Displacement Sensor [Panasonic, Osaka, Japan]. A schematic of the measurement setup, nozzle-substrate pathway and image of a sample produced from experiment setup is shown in Figure 2 (a), (b), and (c), respectively. Resultant substrate curvature due to film stress was measured using a VR3000 wide-area 3D measurement system [Keyence Corp. of America, Itasca, IL] and used to compute the residual stress within the film using Stoney's equation [ref]

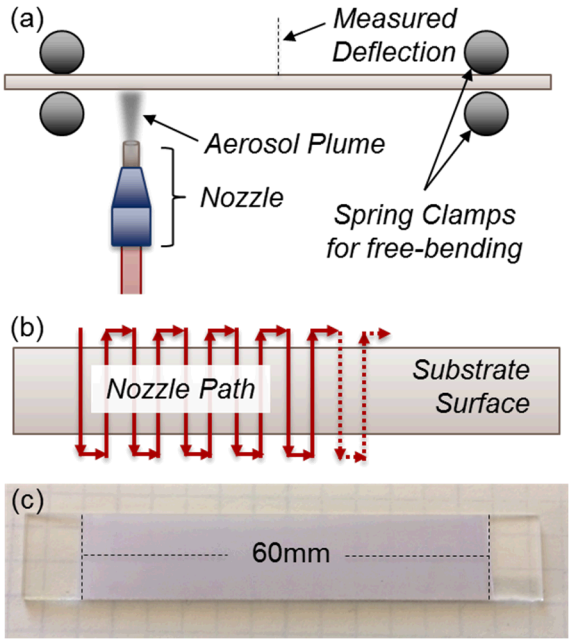

Figure 2: (a) Schematic of the experimental set up to measure the center point deflection of the substrate during aerosol deposition. (b) Nozzle pathway relative to the substrate for film deposition. (c) Film deposited on 60mm length of soda-lime glass substrate

2.2 XRD

XRD phase detection and grain size measurement during heat treatment was carried out using a Scintag Theta-Theta diffractometer with a Cu tube at 40kV and 30mA. Measurements were carried out over a 2θ of 20°-60° at 1.5s per 0.05° interval. Measurements were taken from room temperature to 1200°C in 25°C increments in a flowing air environment. Diffraction patterns were measured again at room temperature after 1200°C heat treatment. Grain size measurements we made from profile fitting of the (110) and (111) $BaTiO_3$ peak

Residual strain of the $BaTiO_3$ films in the as-deposited and post heat treated states were measured by a D8 Discover micro-diffractometer [Bruker, Madison, WI] equipped with a Vantec-2000 2D detector, employing a Cu tube at 40kV, 40mA.

2.3 TEM

3. Results and Discussion

3.1 Phase Composition

The phase composition of the as-received powder, as-deposited film, and 1200°C heat treated film was measured by XRD and are shown in Figure 3. Both the as-received powder and as-deposited films indicate strong peaks of $BaTiO_3$, with small peak intensities corresponding to $BaCO_3$. Using the relative peak intensities, it was found that the amount of $BaCO_3$ was ~3wt% of the as-received powder's and as-deposited film's composition. This indicates that no phase decomposition of the $BaTiO_3$ occurred during deposition and that the propensity for $BaCO_3$ deposited was nearly the same as for the $BaTiO_3$. With the heat treated films, the $BaTiO_3$ peaks narrow and intensify, owing to stress relief and grain growth, while the $BaCo_3$ peaks are no longer detected. Instead, new peaks emerge corresponding to Ba_2TiO_4. With the comparison of peak intensities, ~23wt% of the heat treated film is composed of the new Ba_2TiO_4 phase.

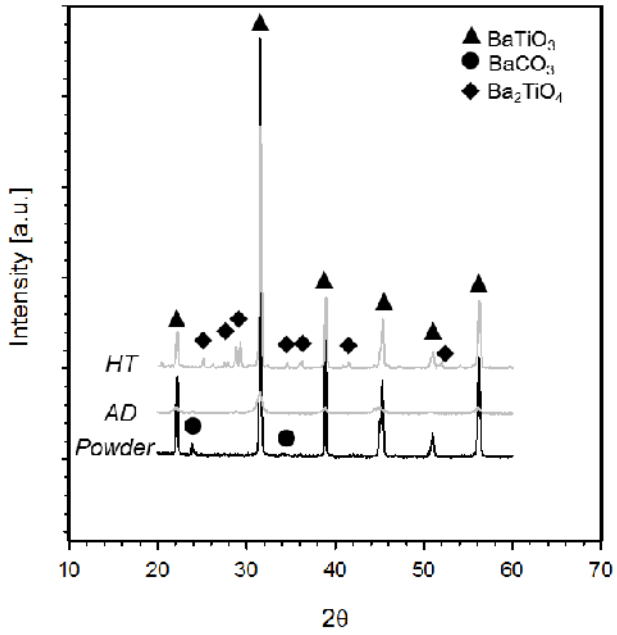

Figure 3: X-Ray Diffraction pattern of the starting powder, as-deposited film, and film heat treated to 1200°C

The XRD diffraction pattern measured throughout the heat treatment is shown in Figure 4, where the loss of the $BaCo_3$ peaks, emergence of Ba_2TiO_4 peaks, and the narrowing and intensifying of the $BaTiO_3$ peaks are easily discerned. The $BaCO_3$ peaks disappear around 700°C, which coincides with the emergence of Ba_2TiO_4 peaks, indicating a transformation of the $BaCO_3$ to Ba_2TiO_4, though no other carbon containing compounds are found throughout the heat treatment. Intensities of both the $BaCo_3$ and Ba_2TiO_4 peaks stay relatively static except for the transition

around 700°C. The $BaTiO_3$ peaks begin to narrow and intensify around 900°C and continue to do so for the remainder of the heat treatment to 1200°C.

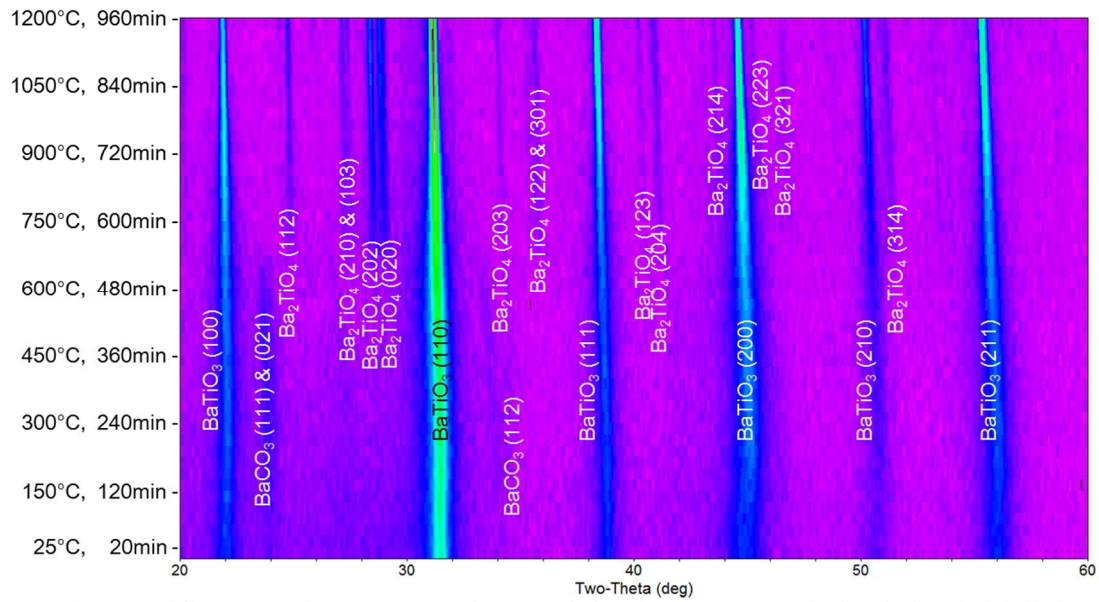

Figure 4: (a) X-ray diffraction peak intensities as a function of 2θ and temperature, with identified peaks labelled. Note the loss of the $BaCo_3$ peak at ~700°C coinciding with the emergence of the Ba_2TiO_4 peak.

3.2 Microstructure and Grain Growth

TEM Microstructure of the as-deposited and heat treated films are shown in Figure 5. The as-deposited film shows a microstructure with very fine grains and a splat-like lamellar structure with few distinguishable particle boundaries. Several horizontally oriented voids are easily observable, indicating regions where complete deformation and bonding of the incoming particles did not occur or were not significantly tamped down by subsequent particle impacts. Similarly, some entrained and largely un-deformed particles are visible within the microstructure. After heat treatment, the microstructure becomes more homogenous, individual grains are observable, and voids take on a more spherical shape. Additionally, XXXX domains become visible in the heat treated microstructure

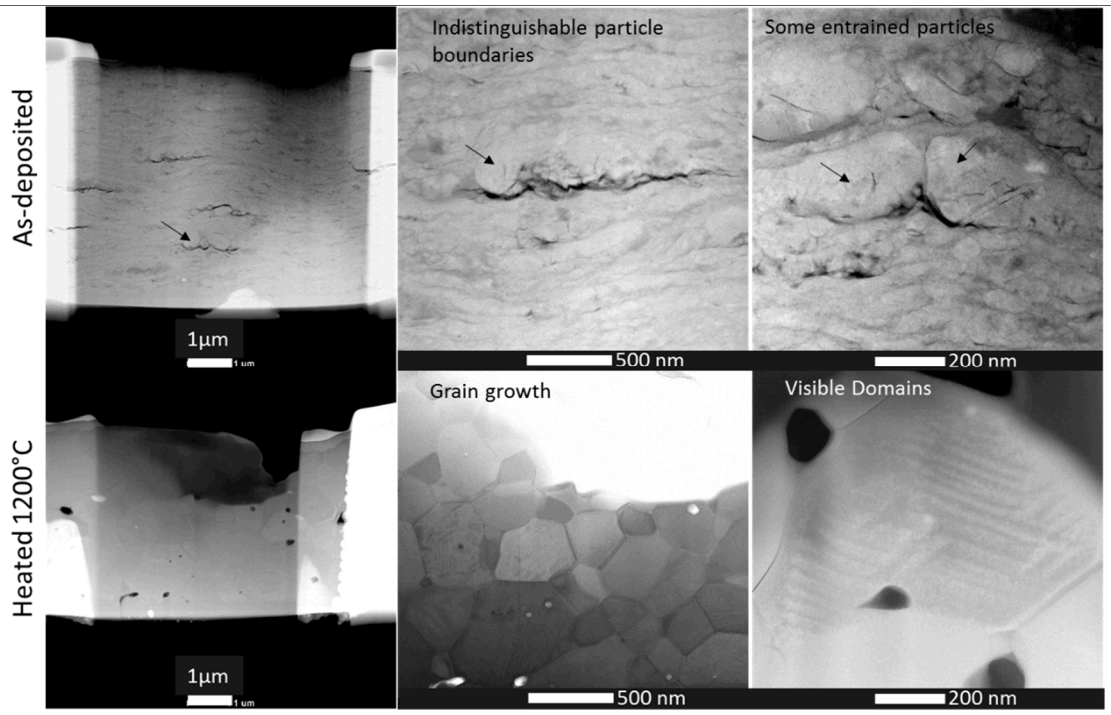

Figure 5: TEM microstructures of the $BaTiO_3$ films in the as-deposited condition and after heat treatment. The as-deposited exhibits very fine grains, with indistinguishable particle boundaries. Defects include some voids and entrained (un-deformed) particles. Well defined grains are present within the heat treated film, as well as visible domains. Some voids are formed during the heat treatment.

The grain size vs. temperature was recorded during the heat treatment of the films, with the results for the (110) and (111) orientations of $BaTiO_3$ shown in Figure 6(a). Grain growth is evident with temperatures great than ~700°C, with a sharp increase at ~900°C. However, during isothermal holds at temperatures where grain growth is expected, there is minimal grain growth over long isothermal holds indicating a stagnation in grain growth as shown in Figure 6(b).

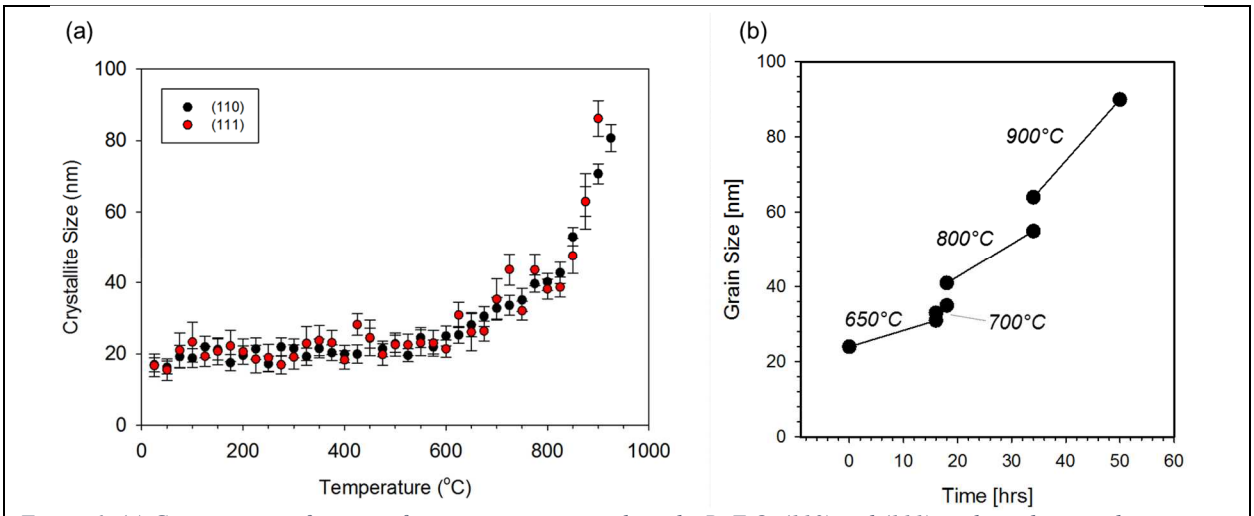

Figure 6: (a) Grain size as a function of temperature measured via the $BaTiO_3$ (110) and (111) peaks, indicating the initiation of grain growth above 600°C. (b) Grain Size of a sample that was held at different temperatures above the onset of grain growth indicated in (a).

TEM imaging of individual grains after 1200°C heat treatment show a segregation of the Ba_2TiO_4 phase towards the grain boundaries, seen in Figure 7. This phase emerged from the decomposition of $BaCo_3$ at ~650°C, leaving behind extra Ba that allowed the formation of the Ba_2TiO_4 phase. This segregation is the cause of the reduced grain growth and low growth rate at temperatures initialing change.

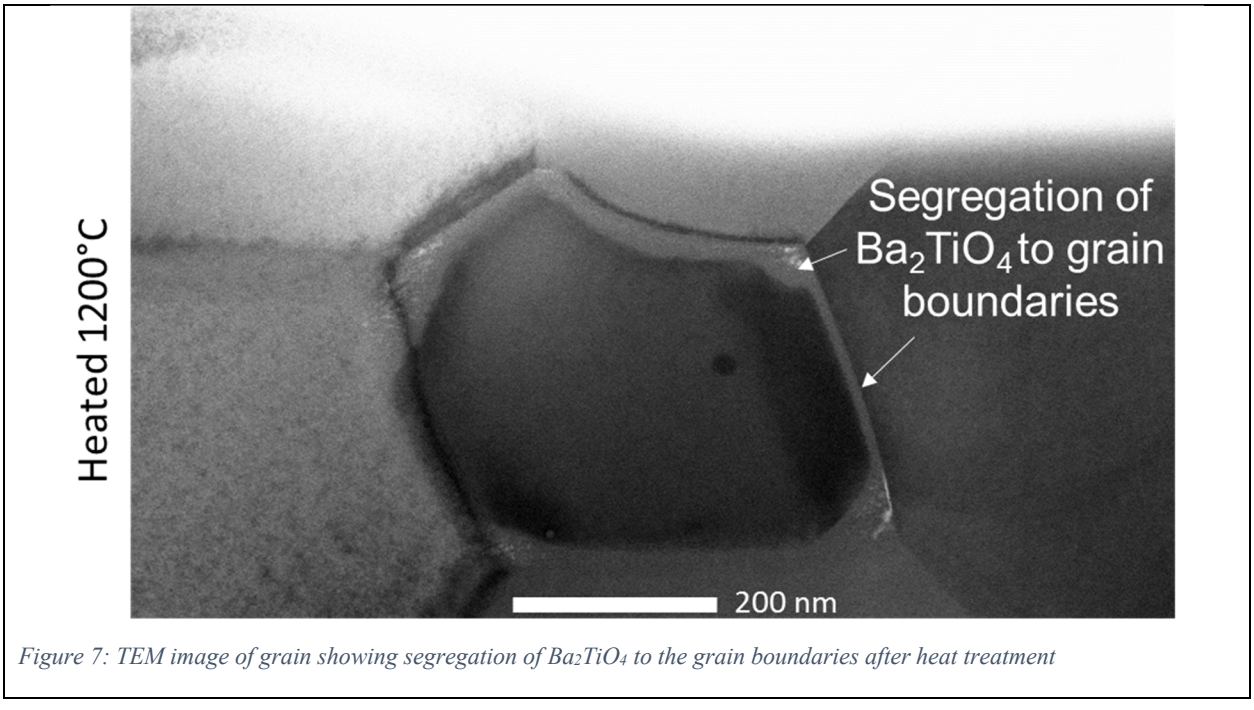

Figure 7: TEM image of grain showing segregation of Ba_2TiO_4 to the grain boundaries after heat treatment

3.3 Residual Stress

The same spray parameters for the heat treatment samples were used to deposit $BaTiO_3$ films onto soda-lime glass substrates in a fixture that allowed free bending of the substrate as the film was deposited, as shown in Figure 2(a). The *in situ* measurement from the laser displacement during the coating deposition was measured at the center point of the substrate and is shown in Figure 8. Three repeat trials were performed, with the absolute values off set to compare the measurement during the spray runs (a portion of Run 3's data signal was lost in the initial deposition passes). The data shows a similar linear slope of deflection vs. time over the course of deposition, with undulations coinciding with each coating pass where a non-uniform bending moment on the substrate occurs until the coating pass is completed through repeated steps (Figure 2(b)).

Coating thickness was measured to be 3,4, and 3.4 µm for runs 1, 2, and 3, respectively. Post deposition measurements were used to calculate the substrate radius of curvature. Using 74 GPa and 0.195 for Modulus and Poisson ratio, respectively, for the soda-lime glass substrate, the residual stress was calculated for each film using the Stoney formula [REF], (inset in Figure 8). Film stress was found to all be compressive with magnitudes of 430, 404, and 507 MPa for runs 1, 2, and 3, respectively.

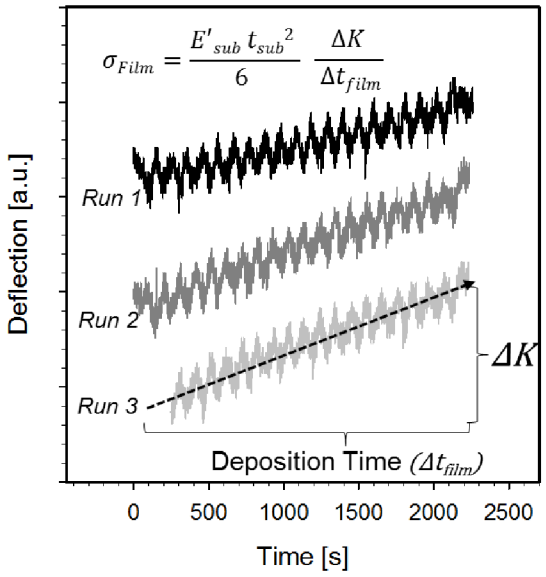

Figure 8: Laser measured displacement during film deposition with three repeat spray trails. A linear relation between accumulation of deflection and coating application is observed, undulations are due to the rastering pattern and successive coating passes to build up coating thickness.

In-situ substrate deflection measurements have been used for stress measurements in other spray coating technologies, such as air plasma spray (APS) [ref SS, kuroda], high velocity oxy-fuel (HVOF) [ref kuroda ss316, me?], and cold spray (CS) [ref varis]. The curvature measurements of these coating technologies typically show similar behavior to what is shown in Figure 8, where a predominantly linear deflection vs. coating application is observed and able to be calculated into

a stress value. The overall linear relationship between deflection change with coating application indicates the coating process to be steady state, with uniform metering of feedstock material and a steady state spectrum of in-flight particle states (temperature, velocity, diameter) resulting in uniform layers of coating microstructure. With the data shown in Figure 8, the AD process indicates behavior of the same manner, where a consistent metering of feedstock, steady state carrier gas and resultant particle state results in consistent deposition behavior of these films. With AD being a room temperature process with no significant substrate heating, there is no further substrate deflection post film deposition whereas APS, HVOF, and CS often have large amounts (10s-100s of MPa) of thermal stress arise from elevated substrate temperatures and thermal expansion mismatches between the coating and substrate.

Residual strain within the as-deposited and 1200°C heat treated films measured by XRD are shown in Figure 9. Strain was measured for the (211) peak, showing a large compressive strain of 0.44% in the as-deposited film. After heat treatment, the (211) peak measure a tensile strain of 0.06% respectively. Using these values, the film stress was calculated to be -572MPa for the as-deposited film and 78MPa for the heat treated film, respectively. Curve fitting of $\Delta d/d°$ vs. $\sin^2(\Psi)$ was limited to a $\Psi°$ tilt of 54 due to a loss in peak quality with further tilt. Pole diagrams of both the as-sprayed and heat treated films showed no preferred grain orientation.

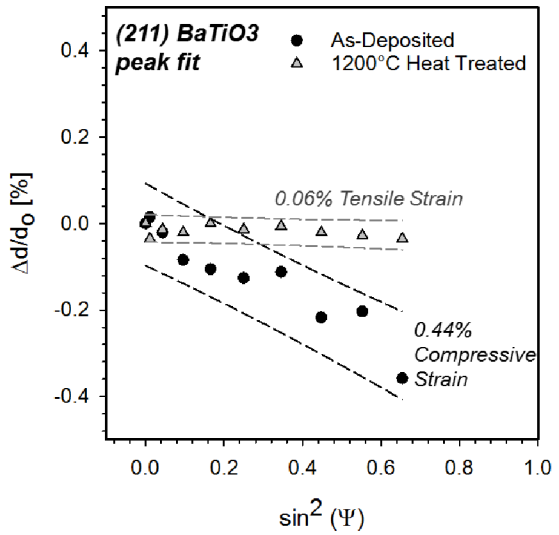

Figure 9: Film strain measured by the sin2 ψ method for $BaTiO_3$ (211) peak before and after heat treatment. The dotted lines indicate the upper and lower prediction intervals.

The values measured for the as-deposited film stress using XRD (572) and Stoney formula (avg. 447 MPa) show both methods to be somewhat comparable, with the stress values being on the same order of magnitude and in compression. However, the samples did have a significant difference in thickness, with 3-4µm of film deposition for the curvature based measurements and 12-13µm of film deposition for the XRD measurements. It is also unknown how the substrate material, sapphire vs. soda lime glass, may have contributed to the film's residual stress state, where the hardness of the substrate may have altered the impact and deformation behavior of

incoming feedstock particles. Literature has used substrate deflection as a method to measure the influence of AD process parameters on film stress, reporting considerable influence of carrier gas mixture on film stress [ref Exner]. Using the same processing parameter for both sapphire and soda lime glass substrates produced comparable film stress states, but the substrate influence requires further study.

With the heat treatment of the film deposited on sapphire, the compressive stress is entirely relieved and a slight tensile stress remains within the film. Examining the top surface of the heat treated films reveals several cracks within the film, shown in Figure 10(a) with a higher magnification image showing more detail of the crack in Figure 10(b). Using reported thermal expansion coefficient from [refs], an estimate of the amount of thermal strain induced in the system upon cool down is ~0.25% for 727°C to from 727 to 20C, leading to the cracking observed in Figure 10. XRD measured strain of the heat treated sample shows the film's tensile stress to be slightly higher than reported tensile fracture values of $BaTiO_3$ [ref], which may be attributed to either the film's fine grain size enhancing its fracture strength [ref] or some un certainty in the XRD measurement. The film stayed adhered to the sapphire substrate while the strain was release through surface cracking, indicating excellent film adhesion to the substrate that was able to resist spallation during heat treatment.

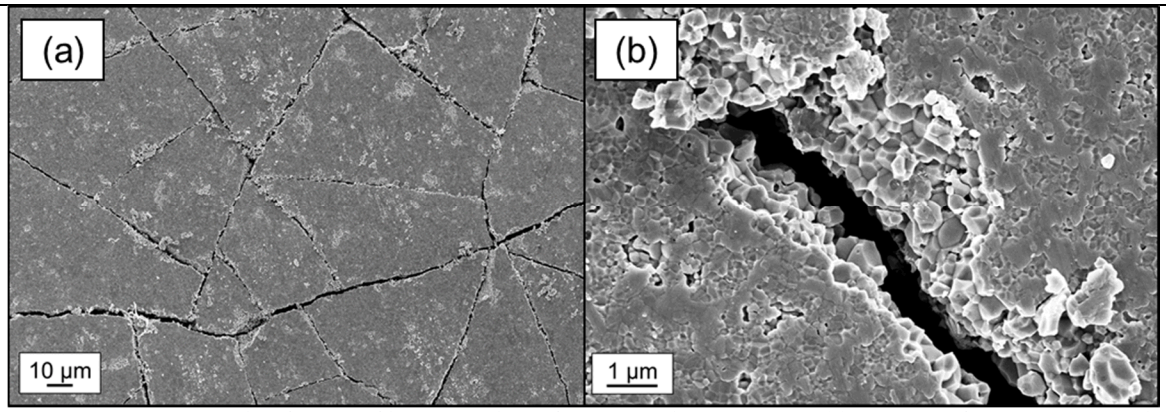

Figure 10: SEM micrographs of $BaTiO_3$ film on Sapphire after 1200°C heat treatment. (a) An array of macroscopic cracks on the film top surface. (b) micrograph of crack showing the grains of the $BaTiO_3$

4. Conclusions

5. Acknowledgements

This work was funded by the Office of Electricity at Sandia National Laboratories

Sandia National Laboratories is a multi-mission laboratory managed and operated by National Technology and Engineering Solutions of Sandia, LLC., a wholly owned subsidiary of

Honeywell International, Inc., for the U.S. Department of Energy's National Nuclear Security Administration under contract DE-NA0003525.

6. References